Block Co-oligomers for Organic Electronics and Optoelectronics: Synthesis, Photophysics, Electroluminescence, and Field-Effect Charge Transport of Oligothiophene-*b*-oligoquinoline-*b*-oligothiophene Triblock Co-oligomers

Jessica M. Hancock, Angela P. Gifford, Richard D. Champion, and Samson A. Jenekhe*

Department of Chemical Engineering and Department of Chemistry, University of Washington, Seattle, Washington 98195-1750

Received February 9, 2008; Revised Manuscript Received March 10, 2008

ABSTRACT: New oligothiophene-*b*-oligoquinoline-*b*-oligothiophene triblock co-oligomers, 6,6′-bis(5-methylthiophenyl-2-yl)-4-phenylquinoline (B1TPQ), 6,6′-bis(2,2′-bithiophenyl-5-yl)-4-phenylquinoline (B2TPQ), and 6,6′-bis(2,2′,5′,2″-terthiophenyl-5-yl)-4-phenylquinoline (B3TPQ), were synthesized, characterized, and found to be efficient blue, green, and yellow emitters in organic light-emitting diodes (OLEDs). The triblock co-oligomers have high fluorescence quantum yields in solution (61−91%), and positive solvatochromism was observed in B2TPQ and B3TPQ. Optical band gaps of evaporated thin films were 2.72 eV (B1TPQ), 2.53 eV (B2TPQ), and 2.27 eV (B3TPQ), indicating strong electronic delocalization over the three blocks of the co-oligomers. Cyclic voltammetry showed reversible reduction in the three triblock co-oligomers from which nearly identical LUMO energies (2.71−2.76 eV) were obtained, implying strong localization of the LUMO on the oligoquinoline middle block. Similarly estimated, the HOMO energy varied from 5.57 eV in B1TPQ to 5.12 eV in B3TPQ and showed strong delocalization of the HOMO across the three blocks of the co-oligomers. Thin films of the co-oligomers showed field-effect charge transport with a hole mobility that varied from 0.7×10^{-5} cm^2/(V s) in B2TPQ to 4.3×10^{-5} cm^2/(V s) in B3TPQ. Bright blue OLEDs based on B1TPQ gave a high luminance (4620 cd/m^2) with a high efficiency (5.6 cd/A, 4.3% EQE). Green OLEDs based on B2TPQ combined high brightness (6535 cd/m^2) with high luminous efficiency (6.5 cd/A). These results provide useful insights for the design and optimization of multicomponent organic/polymer semiconductors for high-performance electronics and optoelectronics.

Introduction

Organic semiconductors are finding diverse applications in organic electronics,[1–10] including organic light-emitting diodes (OLEDs),[1,2] organic field-effect transistors (OFETs),[1,3] and photovoltaic cells.[1,4] Organic semiconductors that have donor−acceptor architectures are proving to be advantageous for organic electronic applications in that they can exhibit (i) ambipolar charge transport in OFETs,[5] (ii) highly efficient electroluminescence due to balanced charge injection and transport in OLEDs,[6–9] and (iii) small band gaps and broad absorption bands of interest in solar cells.[4,10] Organic semiconductors with block copolymer and co-oligomer architectures offer the potential to further fine-tune their electronic and optoelectronic properties for improved devices. Indeed, block conjugated copolymers in which all the sequences are π-conjugated have been of theoretical[11] and experimental[12] interest for quite some time. Besides the expected improved synthetic control and manipulation of the electronic and optical properties, such block conjugated copolymers are also predicted to exhibit novel properties not found in homopolymers or random copolymers due to *electronic localization phenomena* and spatial confinement effects on excitons and carriers.[11–13] Few experimental examples of block conjugated copolymers and co-oligomers are available for exploring these properties and phenomena.[11–13]

In this paper we report the synthesis and properties of new triblock conjugated co-oligomers, oligothiophene-*b*-oligoquinoline-*b*-oligothiophene. The molecular structures of the triblock co-oligomers, 6,6′-bis(5-methylthiophenyl-2-yl)-4-phenylquinoline (B1TPQ), 6,6′-bis(2,2′-bithiophenyl-5-yl)-4-phenylquinoline (B2TPQ), and 6,6′-bis(2,2′,5′,2″-terthiophenyl-5-yl)-4-phenylquinoline (B3TPQ), are shown in Chart 1. The series of co-oligomers has a donor−acceptor−donor triblock architecture and facilitates a study of the effects of block length on the evolution of the electronic structure and properties. The block co-oligomers could also enable elucidation of electronic localization/delocalization phenomena, including intramolecular charge transfer,[14a,c] charge transport,[5] and size effects[14b] on electroluminescence. The solution and solid-state photophysical properties of the co-oligomers were investigated by optical absorption and photoluminescence (PL) spectroscopies. The electronic structure parameters, including the ionization potential (IP/HOMO) and electron affinity (EA/LUMO), were determined by cyclic voltammetry. Charge transport was measured by using the field-effect transistor platform. Additionally, the triblock co-oligomers were explored as emissive materials in OLEDs and found to exhibit highly efficient blue, green, and yellow electroluminescence.

Results and Discussion

Synthesis and Characterization. Scheme 1 shows the synthesis of the block co-oligomers, B*n*TPQ. The desired products were obtained by an acid-catalyzed Friedlander condensation reaction of 3,3′-dibenzoylbenzidine with 5-acetyl-oligothiophene in 68−75% yields. The diphenyl phosphate (DPP) catalyst was readily removed by precipitation into a 10% triethylamine/ethanol solution. B1TPQ was recrystallized in $CHCl_3$, whereas B2TPQ and B3TPQ were recrystallized in THF/MeOH mixtures. ^{1}H NMR, high-resolution mass spectrometry (HRMS), and FTIR were used to confirm the structures of the co-oligomers. The electrochemical and photophysical properties discussed later also confirmed the molecular structures of these compounds.

Differential scanning calorimetry (DSC) of the triblock co-oligomers showed robust thermal resistance characteristics. The

* E-mail: jenekhe@u.washington.edu.

10.1021/ma800304m CCC: $40.75
Published on Web 05/06/2008

Chart 1

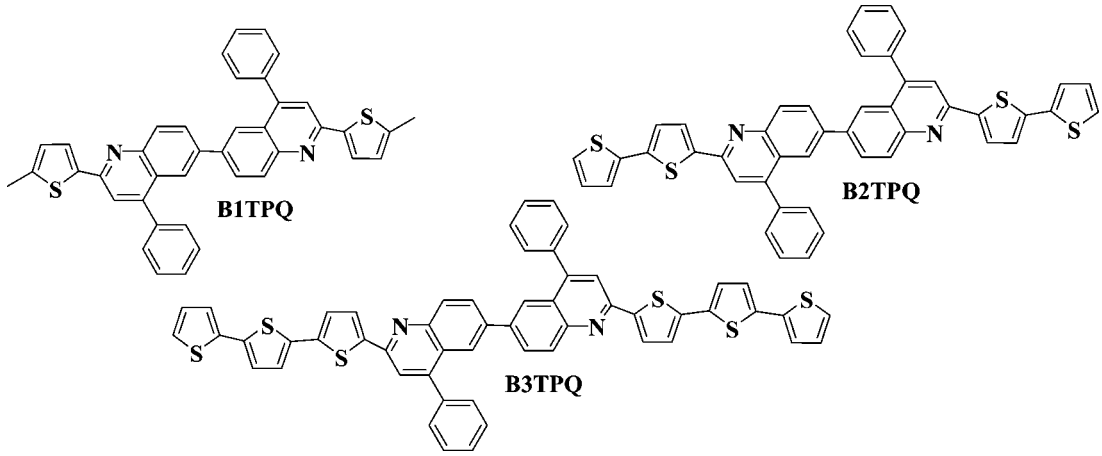

Scheme 1

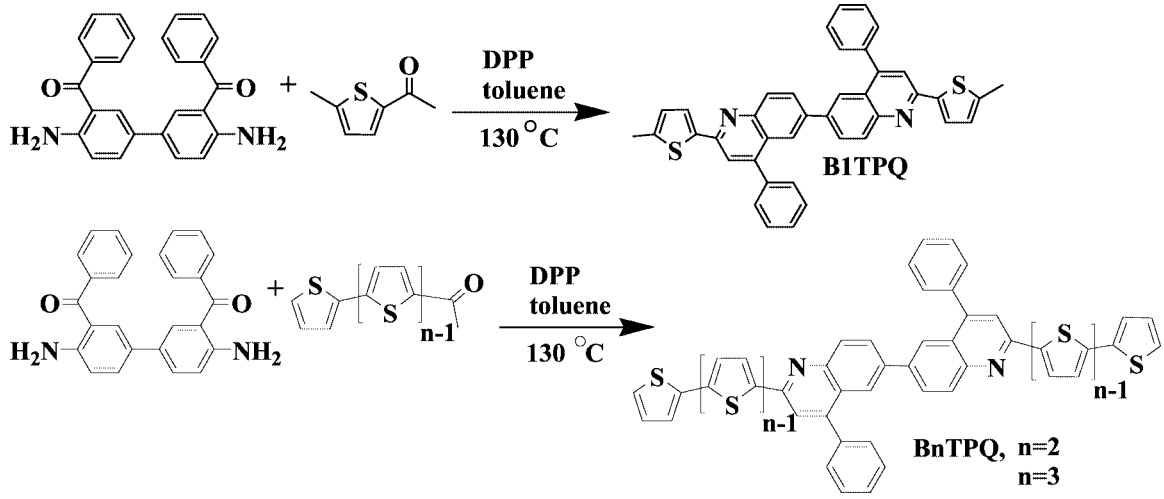

second-heating DSC scan of B1TPQ revealed three distinct transistions: a glass transition (T_g) at 102 °C, a melting transition (T_m) at 259 °C, and an exothermic crystallization peak at 184 °C. The larger oligothiophene blocks in B2TPQ and B3TPQ resulted in higher melting temperatures of 337 and 324 °C, respectively. Clear glass temperatures were not observed. Upon cooling, B3TPQ exhibited an exothermic crystallization peak at 234 °C. Thermogravimetric analysis (TGA) showed that the onset decomposition temperature (T_D) of the co-oligomers was quite high: 461 °C for B1TPQ, 471 °C for B2TPQ, and 462 °C for B3TPQ. The high decomposition temperatures and overall robust thermal resistance properties of these oligomers are in accord with the known features of oligoquinolines[9] and polyquinolines.[15] The oligoquinoline blocks have thus provided the high thermal stability to the co-oligomers (T_m = 259−337 °C) as the T_m of each co-oligomer exceeds those of the constituent oligothiophene blocks (α-2T, T_m = 36 °C and α-3T, T_m = 97 °C).[16] In the case of B2TPQ and B3TPQ, the melting transition even exceeds those of the α-quarterthiophene (α-4T, T_m = 221 °C) and α-sexithiophene (α-6T, T_m = 316 °C).[16]

Electrochemical Properties. The electronic states (HOMO/LUMO levels) of the triblock co-oligomers (B*n*TPQ) were investigated by cyclic voltammetry (CV) to elucidate their redox properties and the potential charge injection processes in devices based on them, such as OLEDs and thin film transistors. The block co-oligomers were not soluble enough in polar organic solvents to do solution CV measurements. The oxidation and reduction cyclic voltammograms of B*n*TPQ thin films on platinum electrodes are shown in Figures 1–3. The electrochemical properties derived from these figures, including oxidation potential (E_{ox}), reduction potential (E_{red}), ionization potential (IP), electron affinity (EA), and electrochemical band gap (E_g^{el}), are summarized in Table 1. The oxidation CVs of the triblock co-oligomers are shown in Figure 1. The oxidation of B1TPQ is characterized by an irreversible wave with a cathodic peak (E_{pc}) at +1.39 V (vs SCE) and an onset oxidation potential (E_{ox}^{onset}) of +1.17 V (vs SCE). An ionization potential (IP) of 5.57 eV was estimated for B1TPQ, using IP = E_{ox}^{onset} + 4.4.[17] Comparison of the oxidation CVs of B2TPQ and B3TPQ to that of B1TPQ reveals two trends: (i) each additional thienyl ring of the oligothiophene blocks generates an additional oxidation wave and (ii) a progressively lower onset oxidation potential with increasing oligothiophene block size. The multiple oxidation waves in B2TPQ (E_{pc} = 1.48, 1.78 V vs SCE) and B3TPQ (E_{pc} = 1.11, 1.40, 1.88 V vs SCE) can be explained as the oxidation of each thiophene ring in the oligomer block at a slightly different potential. These values are in agreement with the oxidation potentials of bithiophene (1.28 V) and terthiophene (1.05 V), and similar size-dependent redox properties have been observed in oligothiophenes.[16,18,19] The lower onset oxidation potential and thus ionization potential of B3TPQ (IP = 5.12 eV) relative to B2TPQ (IP = 5.48 eV) and B1TPQ (IP = 5.57 eV) are expected from the increased electronic delocalization with increasing chain length of the oligothiophene block.[16,18,19] The oxidation CV of B3TPQ, when scanned to 1.6 V (Figure 2), reveals two reversible oxidation waves with formal potentials ($E_{ox}^{o'}$) of 0.97 and 1.28 V. The third oxidation wave of B3TPQ

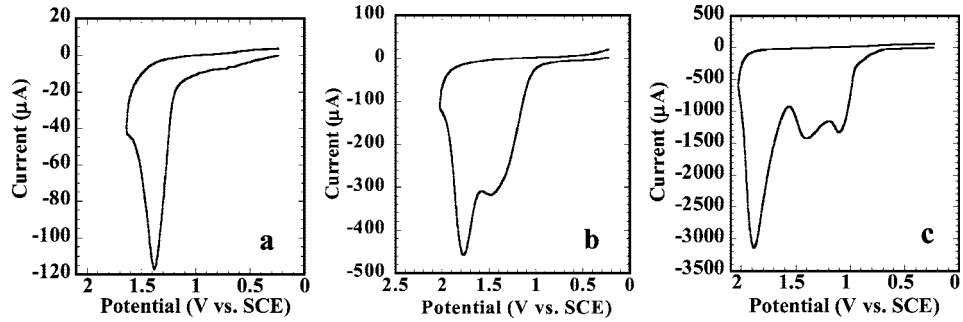

Figure 1. Oxidation cyclic voltammograms of B1TPQ (a), B2TPQ (b), and B3TPQ (c) thin films on platinum wires; scan rate = 60 mV/s.

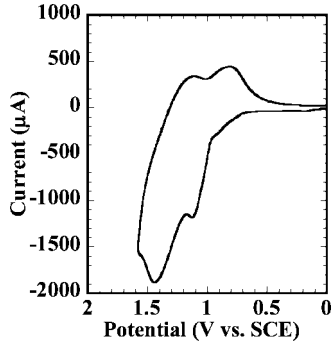

Figure 2. Oxidation cyclic voltammogram of a B3TPQ film on platinum wire scanned from 0 to 1.6 V; scan rate = 60 mV/s.

(E_{pc} = 1.88 V) appears to be overoxidization of the oligothiophene (Figure 1c), and hence reversibility is not observed.

The reduction CVs of the block co-oligomers are shown in Figure 3. The reduction waves are nearly identical due to their identical oligoquinoline block. The reduction CVs of B1TPQ and B3TPQ show two overlapping reversible reduction waves whereas only one reduction wave was observed in B2TPQ. This difference between the three block co-oligomers is likely a consequence of differences in thin film morphology. The onset reduction potentials (E_{red}^{onset}) of the co-oligomers were very similar, −1.69 to −1.64 V vs SCE. The formal reduction potentials ($E_{red}^{o'}$ = −1.77 V for B1TPQ, −1.83 V for B2TPQ, and −1.81 V for B3PPQ) were similarly very close. These values are close to the reported reduction potential of bisphenylquinoline (2-PQ) ($E_{1/2}$ = −1.99 V),[20] confirming that the major contribution to the LUMO level is from the oligoquinoline block. The observed two reduction waves (Figure 3) represent the reduction of each phenylquinoline at a slightly different potential. Similar reduction redox properties have been observed in other oligoquinolines.[9,20] The electron affinity (EA) values or LUMO levels, estimated from the onset reduction potential of the first reduction wave (EA = E_{red}^{onset} + 4.4),[17] are very close for B1TPQ, B2TPQ, and B3TPQ, 2.71−2.76 eV (Table 1).

The IP and EA values were used to calculate the electrochemical band gaps (E_g^{el} = IP − EA) of the block co-oligomers and were found to be 2.41−2.81 eV (Table 1). These results demonstrate band structure engineering, i.e., tuning the HOMO/LUMO levels and band gap of the co-oligomers by choice of the donor and acceptor blocks and the block lengths. It is noteworthy that the similarity of the EA values (2.71−2.76 eV) of all three block co-oligomers provides evidence of strong *electronic localization* of the acceptor middle block. However, since the EA values of the block co-oligomers are 0.3 eV larger than the isolated oligoquinoline (2-PQ, EA = −1.99 V + 4.4 = 2.5 eV), there is some electronic delocalization of the LUMO between the middle oligoquinoline block and the oligothiophene outside block. Indeed, there is an even stronger delocalization of the HOMO between the three blocks given the large disparity between the HOMO level (IP) of the co-oligomers (e.g., 5.12 eV for B3TPQ) and the isolated oligothiophenes (e.g., 5.91 eV for the α-terthiophene, α-3T).[18] This means that holes would be more easily injected into and more stable in the triblock co-oligomers than in the corresponding isolated oligothiophene. Similarly, the larger EA values mean that electron injection into and transport in the block co-oligomers would be much easier than the corresponding parent oligoquinoline and oligothiophene.

Photophysical Properties. Figure 4 shows the normalized optical absorption and photoluminescence (PL) emission spectra of the block co-oligomers in dilute ((4−5) × 10^{-6} M) chloroform solutions and as thin films. The photophysical properties of the co-oligomers, including absorption maxima (λ_{max}^{abs}), molar absorption coefficient (ε), optical band gap (E_g^{opt}), PL emission maximum (λ_{max}^{em}), fluorescence quantum yield (Φ_f), and Commission Internationale d'Eclairage (CIE) coordinates (x,y) are summarized in Table 2. In chloroform solution, B1TPQ displayed a $\pi-\pi^*$ absorption band at 375 nm (log ε = 4.58) and a higher energy band at 293 nm (log ε = 4.67) (Figure 4a). These values are very close to the observed absorption maxima in the phenyl end-capped bisphenylquinoline (B1PPQ) (λ_{max}^{abs} = 356 and 280 nm) and other previously studied oligoquinolines with weak electron-donating end groups (λ_{max}^{abs} = 356−373 nm).[9b,d] The solution absorption spectra of B2TPQ and B3TPQ triblock co-oligomers had absorption maxima at 415 nm (log ε = 5.15) and 436 nm (log ε = 5.08), respectively. The absorption bands of B2TPQ and B3TPQ are considerably red-shifted relative to the $\pi-\pi^*$ bands of oligoquinolines (356−373 nm)[9b,d] and those of the oligothiophenes: bithiophene (302 nm) or α-terthiophene (355 nm).[16,18] These absorption bands of the B2TPQ and B3TPQ co-oligomers can be assigned to charge transfer states, arising from intramolecular charge transfer (ICT) between the acceptor oligoquinoline and donor oligothiophene blocks.[14a] Further confirmation of this assignment comes from solvatochromic shifts in the corresponding PL emission spectra to be discussed below.

The absorption spectra of thermally evaporated thin films of the block co-oligomers have similar line shapes as the solution state absorption spectra (Figure 4c). B1TPQ thin films have absorption maxima at 301 and 392 nm, which represents a 8−17 nm red shift relative to the solution data. A similar red shift of the thin film absorption spectra of B2TPQ (17 nm) and B3TPQ (18 nm) was observed relative to the solution data, indicating an increase in electron delocalization in the solid state relative to dilute solution (Table 2). The solution and solid state absorption spectra of the triblock co-oligomers show clear evidence of electronic delocalization across the constituent oligoquinoline and oligothiophene blocks. First, the absorption spectra are not superposition of those of the constituent oligoquinoline and oligothiophene blocks as would be expected if strong electronic localization occurred; in fact, absorption features characteristic of the constituent π-conjugated oligomers were not observed in the spectra of the co-oligomers. Second,

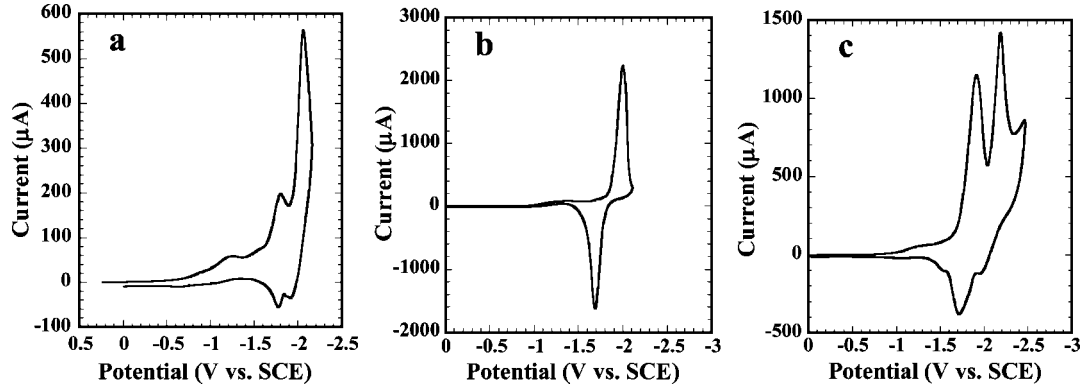

Figure 3. Reduction cyclic voltammograms of B1TPQ (a), B2TPQ (b), and B3TPQ (c) thin films on platinum wires at a scan rate of 60 mV/s.

Table 1. Electrochemical Properties of B*n*TPQ Block Co-oligomers

	E_{ox} [V]	E_{red} [V]	IP [eV]	EA [eV]	E_g^{el} [eV]
B1TPQ	1.17	−1.64	5.57	2.76	2.81
B2TPQ	1.08	−1.66	5.48	2.74	2.74
B3TPQ	0.72	−1.69	5.12	2.71	2.41

the absorption maximum of each co-oligomer exceeds those of the constituent oligomer blocks and even exceeds those of the α-quarterthiophene (α-4T, 391 nm) and α-sexithiophene (α-6T, 436 nm).[16,18] B3TPQ has a relatively small optical band gap of 2.27 eV, calculated from the absorption band edge, whereas B1TPQ and B2TPQ have an E_g^{opt} of 2.72 and 2.53 eV, respectively. These optical band gaps (E_g^{opt}) are 0.09−0.21 eV smaller than the measured electrochemical band gaps (E_g^{el}).

The photoluminescence (PL) emission spectra of B*n*TPQ co-oligomers in chloroform solution are shown in Figure 4b. B1TPQ and B2TPQ emit blue fluorescence with CIE coordinates of (0.16, 0.08) and (0.15, 0.17), respectively. The PL emission

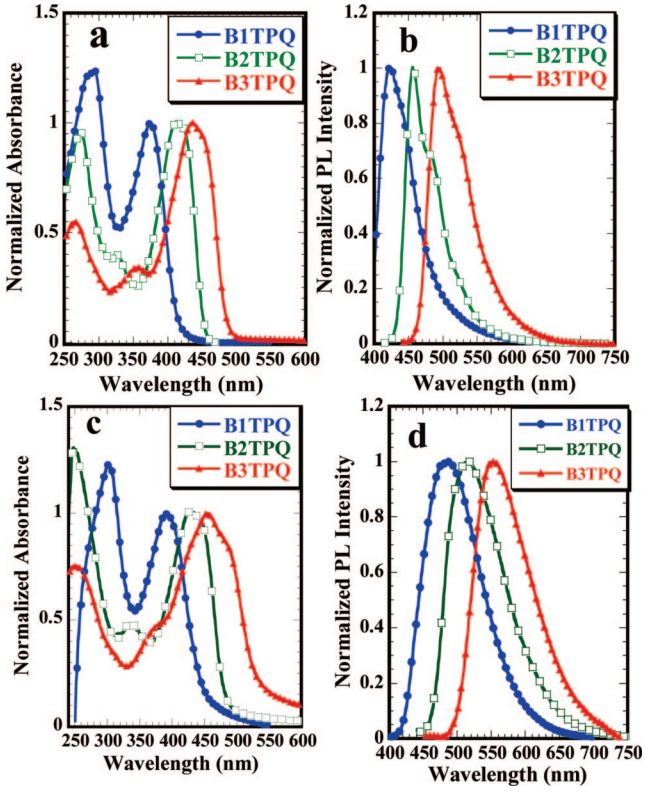

Figure 4. Normalized optical absorption (a) and PL emission (b) spectra of B*n*TPQ block co-oligomers in chloroform. Normalized optical absorption (c) and PL emission (d) spectra of B*n*TPQ as thin films.

of B1TPQ has a maximum (λ_{max}^{em}) at 425 nm and a quantum yield (Φ_f) of 91%. The PL emission spectrum of B1TPQ is similar to that of B1PPQ (λ_{max}^{em} = 401 nm)[9a] and other previously studied oligoquinolines, which have a PL emission maximum of 401−411 nm and quantum yields of 73−94%.[9b,d] The PL emission maximum of B2TPQ is 456 nm with a shoulder at 481 nm and a Φ_f of 74%. B3TPQ emits in the green region (λ_{max}^{em} = 495 nm; CIE (0.22, 0.54)) with a Φ_f of 61%. The decrease of quantum yields from B1TPQ (91%) to B2TPQ (74%) to B3TPQ (61%) can be explained by the increasing intramolecular charge transfer strength with increasing oligothiophene block size in the co-oligomers.[14a]

The PL emission spectra of thin films of B*n*TPQ co-oligomers, shown in Figure 4d, are relatively broad and featureless compared to the solution results. The thin film PL emission spectra of most π-conjugated oligomers and polymers are generally red-shifted from the solution spectra due to changes in conformation.[9] The pure blue PL emission of B1TPQ in solution is shifted to blue-green in the solid state with an emission maximum centered at 486 nm and CIE coordinates of (0.19, 0.32). Similarly, the solid state PL emission spectra of B2TPQ and B3TPQ are further shifted into the green/yellow and yellow/orange regions with bands centered at 518 nm (CIE (0.30, 0.55)) and 552 nm (CIE (0.44, 0.54)), respectively. The red shift of the thin film PL emission spectra of the triblock co-oligomers relative to the solution spectra is consistent with the observed similar red shift in the absorption spectra; both are consequences of the improved electronic delocalization in the solid state and intermolecular interaction induced conformation changes.

Figure 5 shows the solution photoluminescence (PL) emission spectra of the co-oligomers in solvents of varying polarity (dielectric constant): toluene (ε' = 2.4), chloroform (ε' = 4.8), dichloromethane (ε' = 9.1), and acetonitrile (ε' = 36.6). The PL emission spectrum of B1TPQ (Figure 5a) is nearly identical in the different solvents, with a λ_{max}^{em} of 422−425 nm and a full width at half-maximum (fwhm) value of 52−59 nm. The PL emission spectrum of B2TPQ in toluene has a vibronic structure with a maximum at 453 nm, a shoulder at 476 nm, and a fwhm of 47 nm. In acetonitrile, the PL line shape broadens with a fwhm of 73 nm, and the PL maximum is 14 nm red-shifted to 467 nm relative to toluene (Figure 5b). The strongest positive solvatochromism was observed in B3TPQ (Figure 5c). In toluene, B3TPQ has an emission maximum of 486 nm and a fwhm of 57 nm. The PL emission spectrum of B3TPQ becomes featureless and broad (fwhm = 124 nm) in acetonitrile, and the emission maximum is red-shifted to 516 nm. The observed solvatochromism in B2TPQ and B3TPQ shows that the oligothiophene blocks, attached to the same oligoquinoline acceptor block, result in a more polar excited state due to strong intramolecular charge transfer. Following photoexcitation, the

Table 2. Photophysical Properties of B*n*TPQ Block Co-oligomers

		λ_{max}^{abs} [nm]	log ε	E_g^{opt} [eV]	λ_{max}^{em} [nm]	Φ_f[c]	CIE 1931 [*x*,*y*]
B1TPQ	$CHCl_3$[a]	293,375	4.67, 4.58		425	0.91	(0.16,0.08)
	thin film[b]	301,392		2.72	486		(0.19,0.32)
B2TPQ	$CHCl_3$	274,415	5.13, 5.15		456	0.74	(0.15,0.17)
	thin film	249,432		2.53	518		(0.30,0.55)
B3TPQ	$CHCl_3$	265,436	4.79, 5.08		495	0.61	(0.22,0.54)
	thin film	252,454		2.27	552		(0.44,0.54)

[a] $(4-5) \times 10^{-6}$ M. [b] 40−55 nm thick. [c] 9,10-Diphenylanthracene ($\Phi_f = 0.93$) was used as a standard.

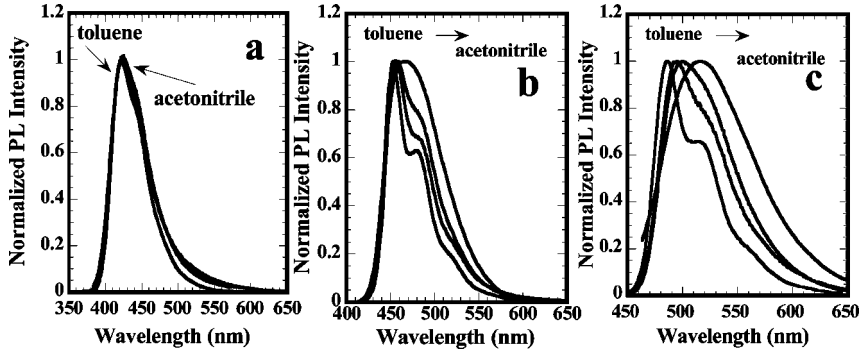

Figure 5. Normalized PL emission spectra of triblock co-oligomers in solvents of varying polarity (toluene, chloroform, dichloromethane, and acetonitrile): B1TPQ (a), B2TPQ (b), and B3TPQ (c).

Table 3. Device Characteristics of OLEDs Based on B*n*TPQ Block Co-oligomers

oligomer	device[a]	V_{on}[b]	drive voltage [V]	current density [*J*, mA/cm^2]	brightness [cd/m^2]	device efficiency[c] [cd/A (% EQE)[d]]	λ_{max}^{EL} [nm]	CIE 1931 [*x*,*y*]
B1TPQ	I	5.8	12.2	34	12	0.03 (0.01)	486	(0.17,0.33)
	II	4.2	10.3	191	2420	5.6 (4.3)	460	(0.15,0.20)
	III	4.3	10.6	158	4620	4.3 (3.3)	450	(0.15,0.19)
	IV	3.5	9.2	213	2990	2.4 (1.9)	453	(0.15,0.19)
	V	4.4	9.4	500	4030	1.7 (1.3)	455	(0.17,0.19)
B2TPQ	I	2.5	8.2	460	110	0.03 (0.01)	474	(0.19,0.27)
	II	4.2	12.0	104	1030	2.2 (0.9)	484	(0.21,0.46)
	III	5.9	15.6	54	2210	6.5 (2.5)	492	(0.20,0.50)
	IV	4.5	10.3	122	2410	2.2 (0.82)	501	(0.23,0.51)
	V	4.8	14.1	433	6535	2.7 (0.99)	497	(0.21,0.48)
B3TPQ	I	2.2	6.3	500	970	0.29 (0.08)	528	(0.39,0.58)
	II	4.3	11.2	500	3330	0.82 (0.23)	528	(0.35,0.61)
	III	4.2	12.2	316	3690	1.3 (0.34)	535	(0.41,0.57)
	IV	2.7	7.9	496	4430	1.1 (0.31)	531	(0.36,0.61)
	V	3.2	8.5	500	3530	0.82 (0.23)	538	(0.37,0.59)

[a] Diode I: ITO/oligomer/LiF/Al; diode II: ITO/PEDOT/PVK/oligomer/LiF/Al; diode III: ITO/PEDOT/PVK/oligomer/TPBI/LiF/Al; diode IV: ITO/PEDOT/TAPC/oligomer/LiF/Al; diode V: ITO/PEDOT/TAPC/oligomer/TPBI/LiF/Al. [b] Turn-on voltage (at which EL is visible to the eyes). [c] Efficiencies are reported at brightness >100 cd/m^2 or the maximum brightness of the diode. [d] EQE = external quantum efficiency.

electrons are more localized on the oligoquinoline block, and the holes are more localized on the oligothiophene blocks.

Electroluminescent Devices. OLEDs of different architectures were fabricated from the triblock co-oligomers and evaluated in ambient air. Five different device structures were investigated: ITO/B*n*TPQ/LiF/Al (diode I), ITO/PEDOT/PVK/B*n*TPQ/LiF/Al (diode II), ITO/PEDOT/PVK/B*n*TPQ/TPBI/LiF/Al (diode III), ITO/PEDOT/TAPC/B*n*TPQ/LiF/Al (diode IV), and ITO/PEDOT/TAPC/B*n*TPQ/TPBI/LiF/Al (diode V). The electroluminescent properties of all the B*n*TPQ-based OLEDs, including the turn-on voltage (V_{on}), drive voltage (V), maximum current density (J_{max}), luminance (*L*), luminous efficiency (cd/A), external quantum efficiency (EQE), and electroluminescence (EL) emission maximum, are summarized in Table 3.

The performance of the single-layer devices (diode I) was poor for both B1TPQ and B2TPQ, obtaining a brightness of 12 and 110 cd/m^2, respectively, and EQEs of 0.01%. The low brightness and current density (34 mA/cm^2) of B1TPQ-based devices indicate poor charge injection into the film. The higher current densities (460 mA/cm^2) in B2TPQ-based diode I suggest improved charge injection, but poor carrier utilization with most of the holes and electrons passing through the device with no recombination. However, markedly good performance was obtained in single-layer OLEDs (diode I) based on B3TPQ, with a low turn-on voltage of 2.2 V and a maximum brightness 970 cd/m^2 at 6.3 V and maximum efficiencies of 0.08% EQE and 0.29 cd/A. These results demonstrate that B3TPQ has more balanced charge injection/transport and efficient charge recombination due to the larger oligothiophene blocks. This interpretation is further supported by the previously discussed ambipolar redox properties and strong intramolecular charge transfer observed in B3TPQ. The EL spectrum line shapes of the B*n*TPQ single-layer devices (diode I) were identical to the PL emission spectrum line shapes of the respective thin films. However, the EL emission maximum in the block co-oligomers at 486 nm (B1TPQ), 474 nm (B2TPQ), and 528 nm (B3TPQ) is either identical to the PL emission maximum (B1TPQ) or blue-shifted by 24−34 nm. Similar shifts between the EL and PL emission spectra of electroluminescent polymers have been reported and have been attributed to conformational changes due to local heating that occurs under the application of an electric field.[21]

The performance of OLEDs based on the B*n*TPQ block co-oligomers as emitters was greatly improved by using additional layers to facilitate the injection, transport, and confinement of

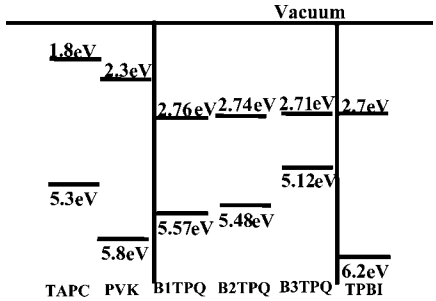

Figure 6. Energy levels (EA/IP) of the emissive triblock co-oligomers and hole or electron-blocking materials (TAPC, PVK, TPBI) used in the OLEDs.

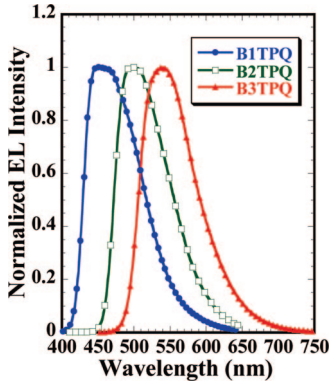

Figure 7. Normalized EL emission spectra of B1TPQ, B2TPQ, and B3TPQ OLEDs at 9, 14, and 8 V, respectively (device V).

electrons and holes (Table 3). An energy-level diagram showing all the HOMO and LUMO levels relevant to the OLEDs is shown in Figure 6. Devices using poly(*N*-vinylcarbazole) (PVK) (diode II) or 1,1-bis(4-tolylaminophenyl)cyclohexane (TAPC) (diode IV) as a hole-transport/electron-blocking layer (HTL) showed turn-on voltages of 2.7−4.5 V, at which uniform emission over the whole pixel was visible to the eye. B1TPQ showed the greatest enhancement in device performance upon the addition of a hole-transporting layer, achieving high efficiencies of 5.6 cd/A and 4.3% EQE in diode II and brightnesses of 2990 cd/m^2 in diode IV. The addition of the HTL facilitates hole injection into the low-lying HOMO level of B1TPQ, which results in more balanced charge injection/transport. However, B3TPQ is the brightest emitter and electron transport material, exhibiting a maximum brightness of 4430 cd/m^2 in diode IV.

Diodes III and V incorporated 1,3,5-tris(*N*-phenylbenzimidizol-2-yl)benzene (TPBI, IP = 6.2−6.7 eV) as a hole-blocking layer (HBL) to confine holes within the emissive block co-oligomer layer. EL spectra of B*n*TPQ-based diode V are shown in Figure 7. The EL emission spectra of diodes III and V were centered at 450−455 nm in B1TPQ, 492−497 nm in B2TPQ, and 535−538 nm in B3TPQ and were nearly identical to the EL emission in diodes II and IV. The EL emission of the triblock co-oligomers in diodes III and V are 17−36 nm blue-shifted relative to their thin film PL maxima. The CIE coordinates of B*n*TPQ electroluminescence from diode V are shown in Figure 8. The variation of the oligothiophene block size in the triblock co-oligomers afforded various EL emission colors, ranging from blue from B1TPQ (CIE(0.17,0.19)) and green from B2TPQ (CIE(0.21,0.48)) to yellow from B3TPQ (CIE(0.37, 0.59)). Typical luminance−current density−voltage characteristics of OLEDs (diode V) made from the triblock co-oligomers are exemplified in Figure 9.

The addition of the TPBI layer did not enhance the efficiencies of B1TPQ- or B3TPQ-based devices. The high EA and IP

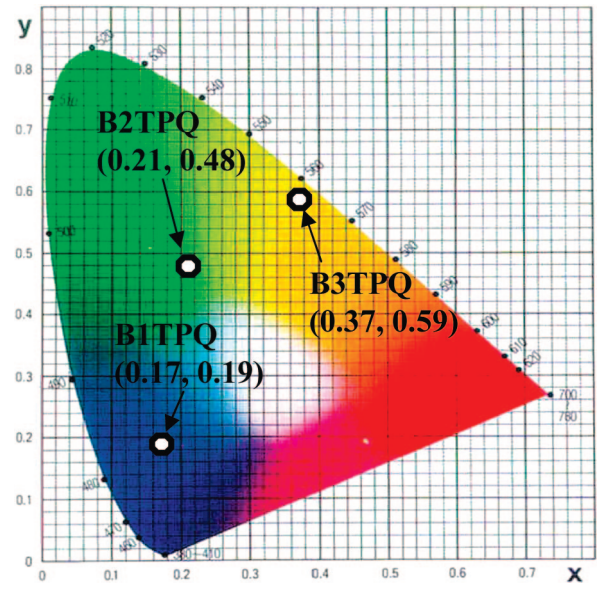

Figure 8. Electroluminescence CIE coordinates of B*n*TPQ triblock co-oligomers (diode V).

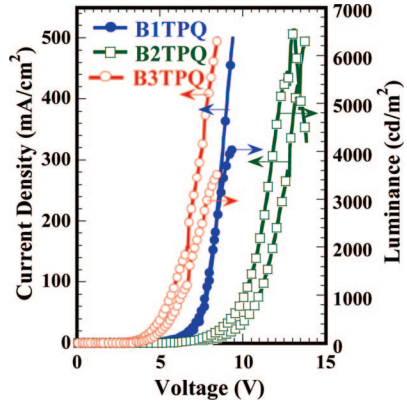

Figure 9. Luminance−current density−voltage characteristics of OLEDs based on B*n*TPQ co-oligomers (diode V).

of B1TPQ afford more effective electron injection/transport; consequently, there is an excess of electrons in the emissive layer. However, the brightness was enhanced by up to 2-fold by the introduction of the TPBI layer (Table 3), which confines the recombination zone within the emissive layer. On the other hand, the lack of enhanced device performance in B3TPQ by introduction of TPBI indicates that it has more balanced charge injection/transport, which is confirmed by the previously discussed ambipolar redox properties and superior single-layer device performance. The most significant enhancement in device performance was observed in B2TPQ-based diode III, with a brightness of 2210 cd/m^2 at 15.6 V and luminous efficiency of 6.5 cd/A and 2.5% EQE. This represents over a 2-fold enhancement in brightness and 2.7-fold increase in device efficiency relative to diode II. B2TPQ-based diode V had the brightest electroluminescence of the series with a luminance of 6535 cd/m^2, due in part to its high fluorescence efficiency (Φ_f = 74%) and efficient charge recombination.

Field-Effect Charge Transport. We used the organic field-effect transistor (OFET) as a platform to explore the charge transport properties of the triblock co-oligomers. All device measurements were done under ambient laboratory conditions. The OFETs showed typical p-channel output characteristics, source-drain current (I_d) vs drain voltage (V_d) at different gate voltages (V_g), under accumulation mode operation. The output

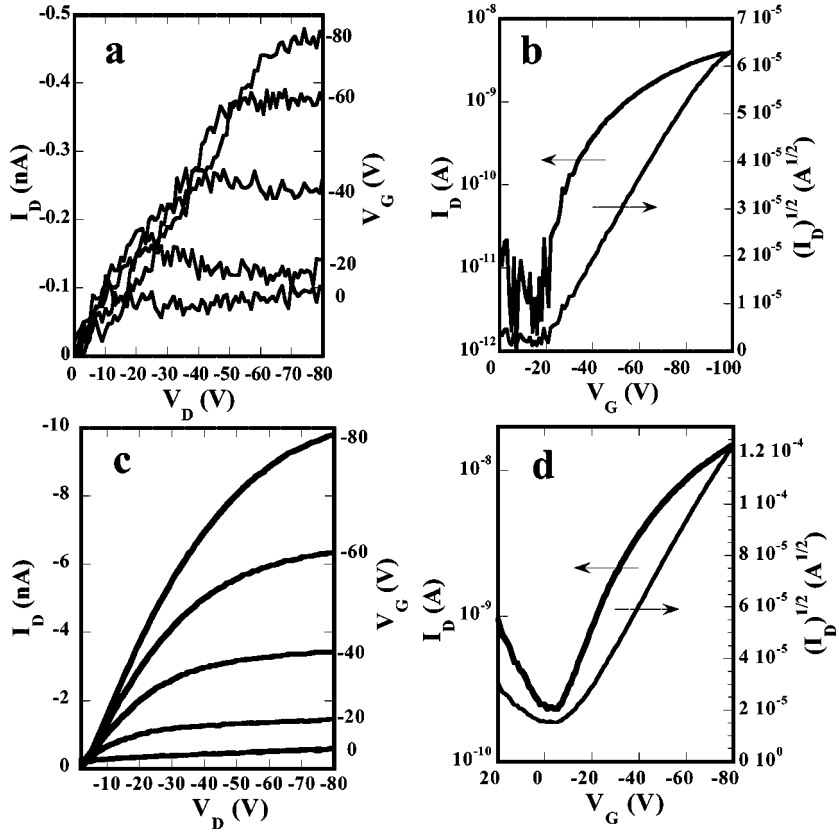

Figure 10. Output and transfer characteristics of B2TPQ (a, b) and B3TPQ (c, d) bottom contact OFETs with OTS-8-treated SiO_2 gate dielectric.

characteristics had good source-drain current modulation and well-defined linear and saturation regions. In the saturation region ($V_d > V_g - V_t$), I_d can be described by the equation[22]

$$I_d = (W/2L)C_0\mu_h(V_g - V_t)^2 \quad (1)$$

where μ_h is the field-effect hole mobility, W is the channel width, L is the channel length, C_0 is the capacitance per unit area of the gate dielectric layer (SiO_2, 300 nm, $C_0 = 11$ nF/cm^2), and V_t is the threshold voltage. The saturation region field-effect mobility was thus calculated from the transfer characteristics of the OFETs by plotting $I_d^{1/2}$ vs V_g.

Thermally evaporated B1TPQ thin films did not show any p- or n-channel OFET characteristics. This can be explained by the inability to achieve either hole or electron injection into B1TPQ (IP = 5.57 eV, EA = 2.76 eV) from the gold source/drain electrodes. Thermally evaporated B2TPQ thin films on untreated SiO_2 dielectric surface had a saturation region hole mobility of 3×10^{-6} cm^2 /(V s) with an I_{on}/I_{off} ratio of 10^2 and a V_t of -23 V. Additional annealing at 100 °C for 10 min improved the I_{on}/I_{off} ratio to 10^3, while the threshold voltage worsened to -33 V. Self-assembled monolayers (SAM) have been shown to promote the molecular chain ordering of organic semiconductors at the gate dielectric/semiconductor interface.[23]Devices with a surface modification of the SiO_2 dielectric by an octyltrichlorosilane (OTS-8) SAM displayed a saturation region hole mobility of 7×10^{-6} cm^2/(V s) with an I_{on}/I_{off} ratio of 10^3 with a V_t of -18 V (Figure 10a,b). B2TPQ had no observable field-effect electron mobility, which can be explained by the high-energy barrier for electron injection from gold ($\Phi \sim 5.1$ eV) to B2TPQ (EA = 2.74 eV).

Improved p-channel charge transport was observed in thermally evaporated B3TPQ thin films, which has the largest oligothiophene blocks. A saturation region hole mobility of 2.5 $\times 10^{-5}$ cm^2/ (V s) with an I_{on}/I_{off} ratio of 10^2 and a V_t of -4 V was observed for B3TPQ on unmodified SiO_2 dielectric. The output and transfer characteristics of B3TPQ OFETs with OTS-8 SAM-treated SiO_2 are shown in Figure 10c,d. A hole mobility of 4.3×10^{-5} cm^2/ (V s), I_{on}/I_{off} ratio of 5×10^2, and a V_t of -6 V were observed. Similar to B2TPQ, B3TPQ had no observable field-effect electron mobility, which can be explained by the high-energy barrier for electron injection from gold into B3TPQ (EA = 2.71 eV).

Since the electron injection and transport properties of all three triblock co-oligomers are similar by virtue of their identical central oligoquinoline block and similar EA of 2.71−2.76 eV, these B*n*TPQ OFET results demonstrate the control of hole injection and transport through the oligothiophene block length. The observed field-effect mobility of holes in B2TPQ (0.7×10^{-5} cm^2/(V s)) and B3TPQ (4.3×10^{-5} cm^2/(V s)) are orders of magnitude lower than in oligothiophene.[24] We note that the thin films used in B*n*TPQ OFETs were thermally evaporated at ambient substrate temperatures whereas organic semiconductors commonly have orders of magnitude higher field-effect mobilities when deposited at 80−120 °C substrate temperatures.[25]Nevertheless, the over 6-fold increase in hole mobility in going from B2TPQ to B3TPQ is important and can also explain the previously discussed superior performance of single-layer OLEDs based on B3TPQ compared to the other block co-oligomers. Finally, our results suggest that in order to achieve ambipolar OFETs from donor−acceptor block co-oligomers or copolymers the HOMO/LUMO energy levels must be suitable for electron/hole injection from the same OFET source/drain electrodes.

Conclusions

We have synthesized and characterized new donor−acceptor triblock co-oligomers, oligothiophene-*b*-oligoquinoline-*b*-oligothiophene, and found that the photophysical and redox proper-

ties as well as their electroluminescence and field-effect charge transport vary significantly with the chain length of the oligothiophene blocks. The co-oligomers had high fluorescence quantum yields in solution, decreasing from 91% in B1TPQ to 61% in B3TPQ with increasing intramolecular charge transfer character. All the triblock co-oligomers showed reversible electrochemical reduction, whereas only B3TPQ had reversible oxidation in cyclic voltammetry. The LUMO energies of the triblock co-oligomers were nearly identical at 2.71−2.76 eV, indicating the strong localization of the LUMO on the oligoquinoline middle block. In contrast, the HOMO energy varied from 5.57 eV in B1TPQ to 5.12 eV in B3TPQ and thus evidence strong delocalization of the HOMO across the three blocks in the co-oligomers. As the emissive materials in OLEDs, blue, green, and yellow electroluminescence was obtained from the block co-oligomers with thiophene (B1TPQ), α-bithiophene (B2TPQ), and α-terthiophene (B3TPQ) outer blocks, respectively. The bright blue OLEDs from B1TPQ had a high luminance (4620 cd/m^2) and a high efficiency (5.6 cd/A, 4.3% EQE). Even higher luminance (6535 cd/m^2) and luminous efficiency (6.5 cd/A) were obtained from the green OLEDs based on B2TPQ. Evaporated thin films of the triblock co-oligomers showed field-effect charge transport with a mobility that varied from 0.7×10^{-5} cm^2/(V s) in B2TPQ to 4.3×10^{-5} cm^2/(V s) in B3TPQ.

Experimental Section

Materials. Diphenyl phosphate (DPP), tetrakis(triphenylphosphine)palladium(0), 2-acetyl-5-methylthiophene, 2-[tributylstannyl]thiophene, 2-acetyl-5-bromothiophene, and 5-(4,4,5,5-tetramethyl-1,3,2-dioxoborolan-2-yl)-2,2′-bithiophene were purchased from Aldrich and used as received. 3,3′-Dibenzoylbenzidine was synthesized according to known literature methods.[26]

Synthetic Procedures. *Synthesis of 1-[2,2′]Bithiophen-5-yl-ethanone.* 4.59 g (12.3 mmol) of 2-[tributylstannyl]thiophene, 2.50 g (12.3 mmol) of 2-acetyl-5-bromothiophene, and 0.300 g (0.26 mmol) of tetrakis(triphenylphosphine)palladium(0) were added to 150 mL of anhydrous toluene under static argon. The reaction mixture was refluxed overnight, and the resulting solution was washed with water, dried with $MgSO_4$, and rotovapped under reduced pressure to concentrate it. The product was separated on a silica gel column using a mixture of 50% CH_2Cl_2/hexanes before recrystallizing with 80% hexanes and 20% CH_2Cl_2 to give 1.83 g of off-white crystals (71% yield). FT-IR (NaCl, cm^{-1}): 3085, 3067, 2387, 1652, 1420, 1360, 1277, 1051, 1036, 1019, 885, 836, 801, 737, 721, 608. GCMS calcd 208.3 for $C_{10}H_8OS_2$; found 208.0.

Synthesis of 1-[2,2′,5′,2″]Terthiophen-5-yl-ethanone. 5.01 g (17.1 mmol) of 5-(4,4,5,5-tetramethyl-1,3,2-dioxoborolan-2-yl)-2,2′-bithiophene, 3.70 g (18.0 mmol) of 2-acetyl-5-bromothiophene, and 0.500 g (0.260 mmol) of tetrakis(triphenylphosphine)palladium(0) were refluxed overnight under Suzuki conditions. The solution was washed with water, dried with $MgSO_4$, and rotovapped under reduced pressure to concentrate it. Resulting product was separated on silica gel column with 50% $CHCl_3$/hexanes mixture to give 3.20 g of yellow-orange crystals (64.4% yield). FT-IR (NaCl, cm^{-1}): 3047, 2985, 2358, 1648, 1560, 1507, 1457, 1443, 1424, 1363, 1296, 1282, 1064, 1034, 867, 836, 793, 720, 668, 649, 634, 610. GCMS calcd 290.4 for $C_{14}H_{10}OS_3$; found 290.0.

General Synthetic Procedure for Co-oligomers. 2.2 equiv of the 5-acetyl-functionalized thieno molecule, 1 equiv of 3,3′-dibenzoylbenzidine, and 5 g of diphenyl phosphate (DPP) were stirred in 3 mL of anhydrous toluene under static argon at 130 °C for 24 h. The reaction mixture was precipitated into 10% triethylamine/ethanol. The precipitate was collected by vacuum filtration, filtered through silica gel to remove polar byproducts, and recrystallized from THF/MeOH mixtures of varying ratios.

6,6′-Bis(5-methylthiophenyl-2-yl)-4-phenylquinoline (B1TPQ). Yield was 75% as a dark yellow crystals. T_m = 259 °C. ^{1}H NMR ($CDCl_3$): δ ppm = 8.24 (s, 1H), 8.23 (s, 1H), 8.13 (d, 2H), 8.03 (d, 1H), 8.00 (d, 1H), 7.70 (s, 2H), 7.57 (m, 10H), 7.38 (d, 2H), 7.01 (d, 2H), 2.68 (s, 6H). FT-IR (NaCl, cm^{-1}): 3056, 3921, 2359, 2341, 1717, 1700, 1684, 1653, 1587, 1573, 1545, 1487, 1436, 1419, 1387, 1216, 1030, 875, 827, 786, 768, 720, 701, 668, 604. HRMS (FAB) calcd 600.8 for $C_{40}H_{28}N_2S_2$; found 600.7.

6,6′-Bis(2,2′-bithiophenyl-5-yl)-4-phenylquinoline (B2TPQ). Yield was 68% as an orange solid. T_m = 337 °C. ^{1}H NMR ($CDCl_3$): δ ppm = 8.23 (s, 1H), 8.22 (s, 1H), 8.14 (d, 2H), 8.03 (d, 1H) 8.02 (d, 1H), 7.71 (s, 2H), 7.58 (m, 10H), 7.37 (m, 6H), 7.31 (d, 2H) 7.10 (d, 2H). FT-IR (NaCl, cm^{-1}): 3386, 3065, 2359, 2319, 1616, 1586, 1560, 1507, 1490, 1465, 1437, 1420, 1363, 1248, 1225, 1073, 878, 841, 826, 796, 767, 697, 668. HRMS (FAB) calcd 737.0 for $C_{46}H_{28}N_2S_4$; found 737.5.

6,6′-Bis(2,2′,5′,2″-terthiophenyl-5-yl)-4-phenylquinoline (B3TPQ). Yield was 72% as reddish-orange solid. T_m = 324 °C. ^{1}H NMR ($CDCl_3$): δ ppm = 8.25 (s, 1H), 8.24 (s, 1H), 8.16 (d, 2H), 8.05 (d, 1H) 8.02 (d, 1H), 7.70 (s, 2H), 7.57 (m, 10H), 7.32 (m, 10H), 7.28 (d, 2H) 7.11 (d, 2H). FT-IR (NaCl, cm^{-1}): 3070, 2916, 2874, 2349, 1704, 1699, 1695, 1675, 1616, 1538, 1462, 1432, 1125, 1077, 880, 826, 795, 694, 666. HRMS (FAB) calcd 901.2 for $C_{54}H_{32}N_2S_6$; found 901.5.

Characterization. FT-IR spectra were taken on a Perkin-Elmer 1720 FTIR spectrophotometer with NaCl plates. ^{1}H NMR spectra were recorded on a Bruker-DRX499 at 500 MHz. DSC analysis was performed on a TA Instruments Q100 differential scanning calorimeter under N_2 at a heating rate of 10 °C/min, and thermogravimetric analysis (TGA) was conducted with a TA Instruments Q50 thermogravimetric analyzer at a heating rate of 10 °C/min under a nitrogen gas flow. UV−vis absorption spectra were recorded on a Perkin-Elmer model Lambda 900 UV/vis/near-IR spectrophotometer. The PL emission spectra were acquired on a Photon Technology International (PTI) Inc. model QM-2001-4 spectrofluorimeter. To measure the PL quantum yields (Φ_f), co-oligomer solutions in spectral grade toluene were prepared. The concentration ($\sim 10^{-6}$ M) was adjusted so that the absorbance of the solution was lower than 0.1. A 10^{-6} M solution of 9,10-diphenylanthracene in toluene (Φ_f = 0.93) was used as a standard.[27]

Cyclic Voltammetry. Cyclic voltammetry experiments were done on an EG&G Princeton Applied Research potentiostat/galvanostat (model 273A). Data were collected and analyzed on the model 270 Electrochemical Analysis System Software on a PC computer. A three-electrode cell was used in all experiments. Platinum wire electrodes were used as both counter and working electrodes and silver/silver ion (Ag in 0.1 M $AgNO_3$ solution, Bioanalytical System, Inc.) was used as a reference electrode. The Ag/Ag^+ ($AgNO_3$) reference electrode was calibrated at the beginning of the experiments by running cyclic voltammetry on ferrocene as the internal standard in an identical cell without any co-oligomer on the working electrode. The films of B*n*TPQ were coated on the Pt working electrode by dipping the Pt wire into a viscous solution in formic acid and subsequently dried in a vacuum oven at 80 °C for 8 h. An electrolyte solution of 0.1 M $TBAPF_6$ in acetonitrile was used in the electrochemical cell. The solution was purged with ultrahigh-purity N_2 for 20 min before the experiment, and a blanket of N_2 was used during the experiment. Electrochemistry was done at a scan rate of 60 mV/s. The block co-oligomers were not soluble enough in polar organic solvents to do solution CV measurements.

Fabrication and Characterization of OLEDs. Indium−tin oxide (ITO)-coated glass substrates (Delta Technologies Ltd., Stillwater, MN) were cleaned sequentially in ultrasonic baths of 2-propanol/deionized water (1:1 volume) mixture, toluene, deionized water, and acetone and then dried at 60 °C in vacuum overnight (~10 h). A 1 wt % poly(ethylenedioxythiophene)/poly(styrenesulfonate) blend (PEDOT) dispersion in water was filtered through a 0.45 μm PVDF syringe filter. A 50 nm thick PEDOT layer was spin-coated onto the ITO-coated glass to act as a hole injection layer and dried at 200 °C for 15 min under vacuum. A 15−20 nm thick hole-transport/electron-blocking layer (HTL) (PVK or TAPC) was spin-coated from its 1 wt % toluene solution onto the PEDOT layer and dried at 60 °C for 4 h under vacuum. A 30−45 nm thick film of each triblock co-oligomer was evaporated from resistively

heated quartz crucibles at a rate of 0.2−0.4 nm/s in a vacuum evaporator (Edwards Auto 306) at a base pressure of $<3 \times 10^{-6}$ Torr onto the HTL layer. For device architectures with a hole blocking layer (diodes III and V), a 15−20 nm thick 1,3,5-tris(*N*-phenylbenzimidizol-2-yl)benzene (TPBI) layer was evaporated onto the triblock co-oligomer. The chamber was vented with air to load the cathode materials, pumped down to $\sim 3 \times 10^{-6}$ Torr, and a 2 nm thick lithium fluoride layer followed by an 120 nm thick aluminum layer were deposited through a shadow mask to form active diode areas of 0.2 cm^2. The film thicknesses were measured by using an Alpha-Step 500 surface profiler (KLA Tencor, Mountain View, CA). Electroluminescence spectra were obtained using a PTI QM-2001-4 spectrophotometer. Current−voltage characteristics of the OLEDs were measured using a HP4155A semiconductor parameter analyzer (Yokogawa Hewlett-Packard, Tokyo). The luminance was simultaneously measured using a model 370 optometer (UDT instruments, Baltamore, MD) equipped with a calibrated luminance sensor head (model 211) and a 5× objective lens. The device external quantum efficiencies were calculated using procedures reported previously.[28]All the device fabrication and characterization steps were done under ambient laboratory conditions.

Surface Modification of SiO_2 Dielectric. The method for depositing a self-assembled monolayer (SAM) on the SiO_2 gate dielectric is similar to a literature method.[29] The flasks and SiO_2/Si OFET substrates were dried in an oven at 120 °C for 20 min. The substrates were immersed in anhydrous toluene under argon at room temperature. Octyltrichlorosilane (OTS-8) was added (10 mM) and left to form a self-assembled monolayer for 1 h under argon. The SAM-treated substrates were removed from the OTS-8 solution, rinsed with anhydrous toluene, and baked at 120 °C for 20 min in an oven. The substrates were sonicated in anhydrous toluene for 1 min and then rinsed further with anhydrous toluene. The OTS-8 SAM-modified OFET substrates were dried in vacuum for 1 h before use.

Fabrication and Characterization of Thin Film Transistors. Bottom-contact geometry was used to fabricate the thin film field-effect transistors. Heavily n-doped Si with a conductivity of 10^3 S/cm was used as a gate electrode with 300 nm thick SiO_2 layer as the gate dielectric. Using photolithography and a vacuum sputtering system (2×10^{-6} Torr), two 90 nm thick gold electrodes (source and drain) with a 10 nm thick adhesive layer of TiW alloy were fabricated onto the SiO_2 layer. A channel length (L) of 25 μm and a channel width (W) of 500 μm were used. The gate electrode launching pad was placed on top of the Si gate electrode after the SiO_2 gate dielectric had been mechanically etched away. On the top of this device structure, thin films (~40 nm) of a co-oligomer was thermally evaporated at a rate of 0.2 nm/s. Electrical characteristics of the devices were measured using a Keithley 4200 semiconductor parameter analyzer (Keithley Instruments, Inc., Cleveland, OH). All the measurements were done under ambient laboratory conditions.

Acknowledgment. This research was supported by the DOE BES (DE-FG02-07ER46467), the NSF STC-MDITR (DMR-0120967), the NSF (CTS-0437912), and an NSF IGERT Nanotechnology Fellowship Award to J.M.H. from the Center of Nanotechnology.

References and Notes

(1) (a) See the special issue on Organic Electronics: *Chem. Mater.* **2004**, *16*, 4381−4846. (b) See the special issue on Organic Electronics and Optoelectronics: *Chem. Rev.* **2007**, *107*, 923−1386.

(2) (a) Tang, C. W.; VanSlyke, S. A. *Appl. Phys. Lett.* **1987**, *51*, 913. (b) Friend, R. H.; Gymer, R. W.; Holmes, A. B.; Burroughs, J. H.; Marks, R. N.; Taliani, C.; Bradley, D. D. C.; Dos Santos, D. A.; Brédas, J. L.; Lögdlund, M.; Salaneck, W. R. *Nature (London)* **1999**, *397*, 121. (c) Kraft, A.; Grimsdale, A. C.; Holmes, A. B. *Angew. Chem., Int. Ed.* **1998**, *37*, 402. (d) Heeger, A. J. *Solid State Commun.* **1998**, *107*, 673. (e) Kulkarni, A. P.; Tonzola, C. J.; Babel, A.; Jenekhe, S. A. *Chem. Mater.* **2004**, *16*, 4556. (f) Hughes, G.; Bryce, M. R. *J. Mater. Chem.* **2005**, *15*, 94. (g) Zhang, X.; Jenekhe, S. A. *Macromolecules* **2000**, *33*, 2069. (h) Chen, C. T. *Chem. Mater.* **2004**, *16*, 4389. (i) Yan, H.; Lee, P.; Armstrong, N. R.; Graham, A.; Evmenenko, G. A.; Dutta, P.; Marks, T. J. *J. Am. Chem. Soc.* **2005**, *127*, 3172. (j) Furuta, P. T.; Deng, L.; Garon, S.; Thompson, M. E.; Frechet, J. M. J. *J. Am. Chem. Soc.* **2004**, *126*, 15388. (k) Forrest, S. R. *Nature (London)* **2004**, *428*, 911. (l) D'Andrade, B. W.; Forrest, S. R. *Adv. Mater.* **2004**, *16*, 1585. (m) Baldo, M. A.; O'Brien, D. F.; You, Y.; Shoustikov, A.; Sibley, S.; Thompson, M. E.; Forrest, S. R. *Nature (London)* **1998**, *395*, 151. (n) Zhu, W.; Mo, Y.; Yuan, M.; Yang, W.; Cao, Y. *Appl. Phys. Lett.* **2002**, *80*, 2045.

(3) (a) Dimitrakopoulos, C. D.; Malenfant, P. R. L. *Adv. Mater.* **2002**, *14*, 99. (b) Bao, Z.; Dodabalapur, A.; Lovinger, A. J. *Appl. Phys. Lett.* **1996**, *69*, 4108. (c) Newman, C. R.; Frisbie, C. D.; Filho, D. A. S.; Brédas, J.-L.; Ewbank, P. C.; Mann, K. R. *Chem. Mater.* **2004**, *16*, 4436. (d) Babel, A.; Jenekhe, S. A. *J. Am. Chem. Soc.* **2003**, *125*, 13656.

(4) (a) Thompson, B. C.; Frechet, J. M. J. *Angew. Chem., Int. Ed.* **2008**, *47*, 58. (b) Gunes, S.; Neugebauer, H.; Sariciftci, N. S. *Chem. Rev.* **2007**, *107*, 1324. (c) Chamberlain, G. A. *Sol. Cells* **1983**, *8*, 47. (d) Wohrle, D.; Meissner, D. *Adv. Mater.* **1991**, *3*, 129. (e) Nunzi, J.-M. *C. R. Phys.* **2002**, *3*, 523. (f) Gregg, B. A. *J. Phys. Chem. B* **2003**, *107*, 4688. (g) Peumans, P.; Yakimov, A.; Forrest, S. R. *J. Appl. Phys.* **2003**, *93*, 3693. (h) Tang, C. W. *Appl. Phys. Lett.* **1986**, *48*, 183. (i) Peumans, P.; Forrest, S. R. *Appl. Phys. Lett.* **2001**, *79*, 126. (j) Yu, G.; Gao, J.; Hummelen, J. C.; Wudl, F.; Heeger, A. J. *Science* **1995**, *270*, 1789. (k) Shaheen, S. E.; Brabec, C. J.; Sariciftci, N. S.; Padinger, F.; Fromherz, T.; Hummelen, J. C. *Appl. Phys. Lett.* **2001**, *78*, 841. (l) Schilinsky, P.; Waldauf, C.; Brabec, C. J. *Appl. Phys. Lett.* **2002**, *81*, 3885. (m) Jenekhe, S. A.; Yi, S. *Appl. Phys. Lett.* **2000**, *77*, 2635. (n) Alam, M. M.; Jenekhe, S. A. *Chem. Mater.* **2004**, *16*, 4647.

(5) (a) Zaumseil, J.; Sirringhaus, H. *Chem. Rev.* **2007**, *107*, 1296. (b) Zaumseil, J.; Donley, C. L.; Kim, J.-S.; Friend, R. H.; Sirringhaus, H. *Adv. Mater.* **2006**, *18*, 2708. (c) Yoon, M.-H.; DiBenedetto, S. A.; Facchetti, A.; Marks, T. J. *J. Am. Chem. Soc.* **2005**, *127*, 1348. (d) Chesterfield, R. J.; Newman, C. R.; Pappenfus, T. M.; Ewbank, P. C.; Haukaas, M. H.; Mann, K. R.; Miller, L. L.; Frisbie, C. D. *Adv. Mater.* **2003**, *15*, 1278. (e) Babel, A.; Wind, J. D.; Jenekhe, S. A. *Adv. Funct. Mater.* **2004**, *14*, 891. (f) Champion, R. D.; Cheng, K.-F.; Pai, C.-L.; Chen, W.-C.; Jenekhe, S. A. *Macromol. Rapid Commun.* **2005**, *26*, 1835. (g) Zhu, Y.; Champion, R. D.; Jenekhe, S. A. *Macromolecules* **2006**, *39*, 8712. (h) Babel, A.; Zhu, Y.; Cheng, K.-F.; Chen, W.-C.; Jenekhe, S. A. *Adv. Funct. Mater.* **2007**, *17*, 2542.

(6) (a) Goes, M.; Verhoeven, J. W.; Hofstraat, H.; Brunner, K. *Chem. Phys. Chem.* **2003**, *4*, 349. (b) Doi, H.; Kinoshita, M.; Okumoto, K.; Shirota, Y. *Chem. Mater.* **2003**, *15*, 1080. (c) Tamoto, N.; Adachi, C.; Nagai, K. *Chem. Mater.* **1997**, *9*, 1077. (d) Chen, S.; Xu, X.; Liu, Y.; Yu, G.; Sun, X.; Qiu, W.; Ma, Y.; Zhu, D. *Adv. Funct. Mater.* **2005**, *15*, 1541. (e) Thompson, B. C.; Madrigal, L. G.; Pinto, M. R.; Kang, T.-S.; Schanze, K. S.; Reynolds, J. R. *J. Polym. Sci., Part A: Polym. Chem.* **2005**, *43*, 1417.

(7) (a) Taranekar, P.; Abdulbaki, M.; Krishnamoorti, R.; Phanichphant, S.; Waenkaew, P.; Patton, D.; Fulghum, T.; Advincula, R. *Macromolecules* **2006**, *39*, 3848. (b) Thomas, K. R. J.; Lin, J. T.; Tao, Y.-T.; Chuen, C.-H. *Chem. Mater.* **2002**, *14*, 3852. (c) Thomas, K. R. J.; Velusamy, M.; Lin, J. T.; Chuen, C.-H.; Tao, Y.-T. *Chem. Mater.* **2005**, *17*, 1860. (d) Thomas, K. R. J.; Lin, J. T.; Velusamy, M.; Tao, Y.-T.; Chuen, C.-H. *Adv. Funct. Mater.* **2004**, *14*, 83.

(8) (a) Kulkarni, A. P.; Zhu, Y.; Jenekhe, S. A. *Macromolecules* **2005**, *38*, 1553. (b) Kulkarni, A. P.; Wu, P.-T.; Kwon, T. W.; Jenekhe, S. A. *J. Phys. Chem. B* **2005**, *109*, 19584. (c) Zhu, Y.; Kulkarni, A. P.; Jenekhe, S. A. *Chem. Mater.* **2005**, *17*, 5225. (d) Kulkarni, A. P.; Kong, X.; Jenekhe, S. A. *Adv. Funct. Mater.* **2006**, *16*, 1057.

(9) (a) Kulkarni, A. P.; Gifford, A. P.; Tonzola, C. J.; Jenekhe, S. A. *Appl. Phys. Lett.* **2005**, *86*, 061106. (b) Tonzola, C. J.; Kulkarni, A. P.; Gifford, A. P.; Kaminsky, W.; Jenekhe, S. A. *Adv. Funct. Mater.* **2007**, *17*, 863. (c) Hancock, J. M.; Gifford, A. P.; Zhu, Y.; Lou, Y.; Jenekhe, S. A. *Chem. Mater.* **2006**, *18*, 4924. (d) Hancock, J. M.; Gifford, A. P.; Tonzola, C. J.; Jenekhe, S. A. *J. Phys. Chem. C* **2007**, *111*, 6875.

(10) (a) Catellani, M.; Luzzati, S.; Lupsac, N.-O.; Raniero, M.; Consonni, R.; Famulari, A.; Meille, S. V.; Giacalone, F.; Segura, J. L.; Martin, N. *J. Mater. Chem.* **2004**, *14*, 67. (b) Winder, C.; Sariciftci, N. S. *J. Mater. Chem.* **2004**, *14*, 1077.

(11) (a) Meyers, F.; Heeger, A. J.; Brédas, J. L. *J. Chem. Phys.* **1992**, *97*, 2750. (b) Alemán, C.; Domingo, V. M.; Fajarí, L.; Juliá, L.; Karpfen, A. *J. Org. Chem.* **1998**, *63*, 1041. (c) Quattrocchi, C.; dos Santos, D. A.; Brédas, J. L. *Synth. Met.* **1995**, *74*, 187. (d) Nobutoki, H.; Koezuka, H. *J. Phys. Chem.* **1996**, *100*, 6451.

(12) (a) Chen, X. L.; Jenekhe, S. A. *Macromolecules* **1996**, *29*, 6189. (b) Yu, W.-L.; Meng, H.; Pei, J.; Huang, W. *J. Am. Chem. Soc.* **1998**, *120*, 11808. (c) Liang, Y.; Wang, H.; Yuan, S.; Lee, Y.; Gan, L.; Yu, L. *J. Mater. Chem.* **2007**, *17*, 2183. (d) Chen, X. L.; Jenekhe, S. A. *Appl. Phys. Lett.* **1997**, *70*, 487. (e) Tu, G.; Li, H.; Forster, M.;

Heiderhoff, R.; Balk, L. J.; Scherf, U. *Macromolecules* **2006**, *39*, 4327. (f) Chen, X. L.; Jenekhe, S. A. *Synth. Met.* **1997**, *85*, 1431.
(13) (a) Wang, H.; Ng, M.-K.; Wang, L.; Yu, L. P.; Lin, B.; Meron, M.; Xiao, Y. *Chem.—Eur. J.* **2002**, *8*, 3246. (b) Grey, J. K.; Kim, D. Y.; Lee, Y. J.; Gutierrez, J. J.; Luong, N.; Ferraris, J. P.; Barbara, P. F. *Angew. Chem., Int. Ed.* **2005**, *44*, 6207.
(14) (a) Jenekhe, S. A.; Lu, L.; Alam, M. M. *Macromolecules* **2001**, *34*, 7315. (b) Jenekhe, S. A.; Zhang, X.; Chen, X. L.; Choong, V.-E.; Gao, Y.; Hsieh, B. R. *Chem. Mater.* **1997**, *9*, 409. (c) Zhu, Y.; Gibbons, K. M.; Kulkarni, A. P.; Jenekhe, S. A. *Macromolecules* **2007**, *40*, 804.
(15) (a) Zhang, X.; Shetty, A. S.; Jenekhe, S. A. *Macromolecules* **1999**, *32*, 7422. (b) Zhu, Y.; Alam, M. M.; Jenekhe, S. A. *Macromolecules* **2003**, *36*, 8958. (c) Tonzola, C. J.; Alam, M. M.; Jenekhe, S. A. *Adv. Mater.* **2002**, *14*, 1086. (d) Tonzola, C. J.; Alam, M. M.; Jenekhe, S. A. *Macromolecules* **2005**, *38*, 9539.
(16) Facchetti, A.; Yoon, M. H.; Stern, C. L.; Hutchison, G. R.; Ratner, M. A.; Marks, T. J. *J. Am. Chem. Soc.* **2004**, *126*, 13480.
(17) Agrawal, A. K.; Jenekhe, S. A. *Chem. Mater.* **1996**, *8*, 579.
(18) *Electronic Materials: The Oligomer Approach*; Mullen, K., Wegner, G., Eds.; Wiley-VCH: Weinheim, Germany, 1998.
(19) (a) Domagala, W.; Laokowski, M.; Guillerez, S.; Bidan, G. *Electrochim. Acta* **2003**, *48*, 2379. (b) Meerholz, K.; Heinze, J. *Electrochim. Acta* **1996**, *41*, 1839. (c) Brédas, J. L.; Silbey, R.; Boudreaux, D. S.; Chance, R. R. *J. Am. Chem. Soc.* **1983**, *105*, 6555.
(20) (a) Lai, R. Y.; Fabrizio, E. F.; Lu, L.; Jenekhe, S. A.; Bard, A. J. *J. Am. Chem. Soc.* **2001**, *123*, 9112. (b) Lai, R. Y.; Kong, X.; Jenekhe, S. A.; Bard, A. J. *J. Am. Chem. Soc.* **2003**, *125*, 12631.
(21) Mikroyannidis, J. A.; Spiliopoulos, I. K.; Kasimis, T. S.; Kulkarni, A. P.; Jenekhe, S. A. *Macromolecules* **2003**, *36*, 9295.
(22) Sze, S. M. *Physics of Semiconductor Devices*; Wiley: New York, 1981.
(23) Salleo, A.; Chabinyc, M. L.; Yang, M. S.; Street, R. A. *Appl. Phys. Lett.* **2002**, *81*, 4383.
(24) (a) *Organic Electronics*; Klauck, H., Ed.; VCH: Weinheim, Germany, 2007. (b) *Organic Field-Effect Transistors*; Bao, Z., Locklin, J., Eds.; CRC Press: Boca Raton, FL, 2007.
(25) (a) Knipp, D.; Street, R. A.; Völkel, A. R.; Ho, J. *J. Appl. Phys.* **2003**, *93*, 347. (b) Knipp, D.; Street, R. A.; Völkel, A. R. *Appl. Phys. Lett.* **2002**, *82*, 3907.
(26) (a) Agrawal, A. K.; Jenekhe, S. A. *Macromolecules* **1993**, *26*, 895. (b) Tonzola, C. J.; Alam, M. M.; Bean, B. A.; Jenekhe, S. A. *Macromolecules* **2004**, *37*, 3554.
(27) Heinrich, G.; Schoof, S.; Gusten, H. *J. Photochem.* **1974**, *3*, 315.
(28) (a) Kulkarni, A. P.; Jenekhe, S. A. *Macromolecules* **2003**, *36*, 5285. (b) Okamoto, S.; Tanaka, K.; Izumi, Y.; Adachi, H.; Yamaji, T.; Suzuki, T. *Jpn. J. Appl. Phys.* **2001**, *40*, L783.
(29) Lee, D. H.; Kim, D.; Oh, T.; Cho, K. *Langmuir* **2004**, *20*, 8124.

MA800304M